Polymer 50 (2009) 6166–6171

Contents lists available at ScienceDirect

Polymer

journal homepage: www.elsevier.com/locate/polymer

Re-assembly behaviors of polystyrene-*b*-poly(acrylic acid) micelles

Yang Zhang [a], Xing Xiao [a], Jian-jun Zhou [a], Lei Wang [a], Zhi-bo Li [a], Lin Li [a,*], Lin-qi Shi [b], Chi-Ming Chan [c]

[a] Institute of Chemistry, Chinese Academy of Sciences, Beijing 100190, China
[b] Key Laboratory of Functional Polymer Materials of Ministry of Education, Institute of Polymer Chemistry, Nankai University, Tianjin 300071, China
[c] Department of Chemical and Biomolecular Engineering, Hong Kong University of Science and Technology, Clear Water Bay, Hong Kong

ARTICLE INFO

Article history:
Received 12 June 2009
Received in revised form
30 September 2009
Accepted 2 October 2009
Available online 23 October 2009

Keywords:
Block copolymers
Micelles
Re-assembly

ABSTRACT

The re-assembly behaviors of spherical micelles of the polystyrene-*b*-poly(acrylic acid) (PS-*b*-PAA) diblock copolymer in different solvent mixtures were investigated using dynamic light scattering, transmission electron microscopy and atomic force microscopy. Depending on the nature of the solvent, PS-*b*-PAA micelles re-assembled from spheres to nanorings in toluene or to necklace-like aggregates in water induced by solvent evaporation. Systematic studies suggested that the re-assembly behaviors on a neutral surface are strongly correlated with the micellar surface components, the solvent polarity and the chain length of the micelle corona of the solvated blocks. We proposed that the formation of nanorings from PS-*b*-PAA micelles in toluene is mainly induced by the dewetting process of the solvent, while the necklace-like structure arises from the hydrogen bonding interactions among the partially dissociated PAA units.

1. Introduction

Self-assembly, which is ubiquitous in chemistry, biology and materials science, can be viewed as a process of spontaneous reorganization from a disordered system to an ordered suprastructure, with or without external stimuli. Self-assembly occurs on multi-length scales, ranging from the sub-nanometer to the micrometer [1]. In addition to naturally occurring self-assembly systems, synthetic amphiphilic block copolymers can self-assemble into a variety of morphologies with advanced functions. Numerous amphiphilic copolymers have been shown to self-assemble into various morphologies, including spheres, rods, vesicles [2], nanotubes [3,4], cylindrical networks [5], lamellar aggregates [6,7] and ordered microporous films [8]. The length scale of these objects can be tuned via changes in the molecular parameters and the selection of different chemical moieties to create further control over the material functions. Most self-assembled block copolymers were achieved via a single step by controlling the solution conditions (e.g., solvent mixture, pH manipulation, salt concentration and temperature) [9–12]. Micellar morphologies were varied either by changing the copolymer composition or the solvent selectivity [13,14]. The mechanisms of self-assembly of block copolymers in selective solvents are well understood [15].

In addition to the one-step method of tuning the self-assembled copolymers, a second process could be used to induce a re-assembly, which can produce more complicated structures. However, little work has been reported on the underlying assembly mechanism and the routes of the morphological control. Recently, Pochan and co-workers described a morphological transformation from spherical micelles to one-dimensional packing by adding divalent organic counterions [16]. Two steps were employed in this self-assembly process. The first step was the transition of spherical micelles into disk-like micelles and the second step was the forced growth of disk-like micelles along a preferred axis via the formation of organic diamine complexation with charged PAA blocks, forming one-dimensional structures. Most recently, Förster et al. reported on the reconstruction of classical micellar morphologies, i.e., spheres, cylinders and vesicles, from polymer coated nanoparticles [17]. The re-assembly from already existing micelles may have involved numerous interactions and complex physical chemistry. As a consequence, we are intrigued by the opportunities to create highly ordered materials with multiple internal compartments and to explore their underlying mechanisms and morphological control. Moreover, the possibility of multiple compartments offers the potential for multi-component drug-delivery applications [18] or as an anti-friction additive in lubricating oils [19].

The morphological control of polystyrene-*block*-poly(acrylic acid) (PS-*b*-PAA) via variation of the copolymer composition or selection of the solvent has been well documented [2,3,20]. However, little work has been reported on the relationship between the chemical constituents of the micellar surface and their corresponding re-assembly behaviors or on the underlying mechanisms. We therefore chose a well-studied PS-*b*-PAA diblock copolymer as a model system and studied its re-assembly behaviors in different selective solvents.

* Corresponding author. Tel./fax: +86 10 82619830.
E-mail address: lilin@iccas.ac.cn (L. Li).

0032-3861/$ – see front matter © 2009 Elsevier Ltd. All rights reserved.
doi:10.1016/j.polymer.2009.10.031

2. Experimental section

2.1. Polymerization

The block copolymer was synthesized by sequentially incorporating *tert*-butyl acrylate (*t*BA) and styrene by atom transfer radical polymerization. The poly-*t*BA (P*t*BA) segment was later converted into poly(acrylic acid) (PAA). The details on the synthesis of PS-*b*-PAA were the same as in a previous study [21]. The number-average molecular weight and the polydispersity of the PS-*b*-PAA copolymer were determined by a combination of gel permeation chromatography (GPC) and ^{1}H NMR. GPC measurements were carried out on a Waters 2414 gel chromatograph using a series of monodispersed polystyrenes as the calibration standard and THF as the eluent with a flow rate of 1.0 mL/min at 40 °C. ^{1}H NMR spectra were obtained on a Bruker AV 400 NMR spectrometer using chloroform-d ($CDCl_3$) as the solvent and tetramethylsilane as the internal standard. The polydispersity index of the PS_{385}-*b*-PAA_{154} copolymer was measured to be 1.18.

2.2. Preparation of micellar solutions

Micelle 1 with PAA as its core and PS as its shell was prepared according to the following procedure. PS_{385}-*b*-PAA_{154} was first dissolved in tetrahydrofuran (THF) to make a 2.0 mg/mL solution. Then, toluene (a precipitant for the PAA blocks) was added slowly to the vigorously stirred copolymer solution to induce micelle formation. The THF was removed by evaporation under reduced pressure. Finally, a given volume of toluene was added to the micellar solution to bring the concentration to 0.20 mg/mL. Similar procedures were adopted for the preparation of the **Micelle 2** solution. PS_{385}-*b*-PAA_{154} was initially dissolved in *N*,*N*-dimethylformamide (DMF) (2.0 mg/mL) followed with slow addition of deionized water into the vigorously stirred copolymer solution to induce self-assembly of the copolymer. The resulting micellar solution was then dialyzed against water for 14 days with the water changed every 6 h to remove the DMF. Finally, a given volume of water was added to the micellar solution to bring the concentration to 0.20 mg/mL.

2.3. Characterization

Dynamic light scattering (DLS) spectra were obtained using a commercial LLS spectrometer (ALV/DLS/SLS-5022F) equipped with a multi-τ digital time correlator (ALV5000) and a cylindrical 22-mW UNIPHASE He–Ne laser ($\lambda_0 = 632.8$ nm). Solutions were filtered through 0.45-μm Millipore filters individually into dust-free light scattering cells. All measurements were carried out at 20 °C and at a detection angle of 90°. Atomic force microscopy (AFM) images were obtained with a Nanoscope III MultiMode scanning probe microscope (Digital Instruments, Santa Barbara, California) in the tapping mode using silicon tips (TESP, Digital Instruments) with a resonance frequency of approximately 300 kHz and a spring constant of about 40 Nm^{-1}. The AFM specimens were prepared by spin-coating the solutions onto newly cleaved highly ordered pyrolytic graphite (HOPG) substrates. The scanned areas were near the center of the substrates. Micrographs were obtained with a JEOL JEM-2200 transmission electron microscope (TEM) operated at an acceleration voltage of 200 kV. TEM specimens were prepared by freeze-drying, and spin-coating methods. Spin-coated samples were prepared on copper grids (precoated with a thin film of poly(vinylformaldehyde) and with carbon) using clean glass slides as substrates. The spin-coated samples were further dried under ambient conditions for 24 h before they were used for experiments. The volume of the solutions pipetted onto HOPG and TEM grids was 5 μL, except for those specifically mentioned.

3. Results and discussion

Following a similar procedure from a previous report [22], we processed PS_{385}-*b*-PAA_{154} in a mixture of THF and toluene followed by evaporation under reduced pressure to remove the THF. The TEM micrograph, as shown in Fig. 1a, reveals that PS_{385}-*b*-PAA_{154} formed spherical micelles (**Micelle 1**) with radius of about 26 nm and the DLS results indicate an average radius of 43 nm (see supporting information, Fig. S1a). The radius determined with DLS is much larger than that determined by TEM because the shells of the micelles are highly extended in the solvent, forming so-called star-like micelles. We then used the spin-coating method to remove the toluene and found that the PS_{385}-*b*-PAA_{154} spherical micelles re-assemble into a mixture of large compound micelles and nanorings (c.f., Fig. 1b and c) when 5 μL solution was used on the TEM grids or on the 6 mm × 6 mm HOPG substrates. We also found that an increase in the volume of the solution from 3 to 10 μL on a same size HOPG substrate led to the formation of more compound micelles and that a decrease in the volume of the solution favored the formation of uniform nanorings.

Ring formation during solvent evaporation has been extensively studied. Several theoretical models have been proposed to explain their formation, including the "breath figures" mechanism [23], mechanical strain [24], broken vesicles in the center [25],

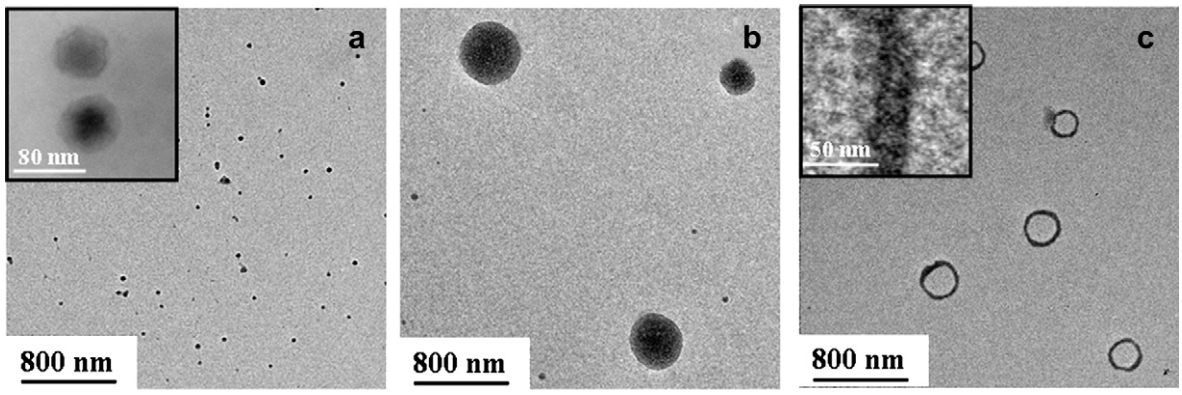

Fig. 1. TEM micrographs showing the re-assembly of **Micelle 1**. (a) Spherical micelles. (b) Large compound micelles. (c) Nanorings. The inset of (a) shows spherical micelles of PS_{385}-*b*-PAA_{154} with PAA as their cores and PS as their shells. The inset of (c) is a high-resolution TEM micrograph of the toroidal perimeter. Samples were prepared (a) using drop-coating method, (b) and (c) using spin-coating method.

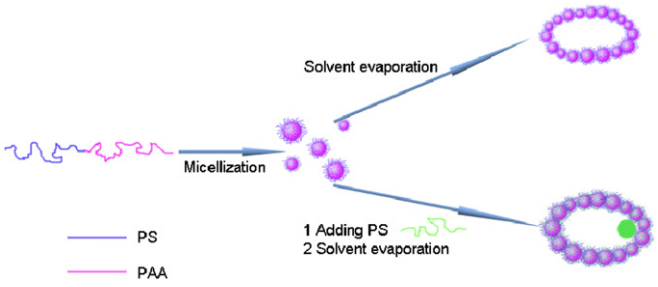

Scheme 1. Schematic representation of the re-assembly of **Micelle 1** into nanorings.

cylindrical micelles end-to-end connection [26], the Marangoni effect [27], the hole-nucleation mechanism [28], "2D gas bubbles" [29], and capillary flow-induced localization along the moving three-phase line [30].

Micelle 1, with PAA blocks as its core and PS blocks as its shell transformed into nanorings and large compound micelles. To explain the observed results, we propose a hole-nucleation and -growth process that occurs during dewetting of the solution films, as illustrated in Scheme 1. The process is as follows: When the **Micelle 1** solution is spread on a carbon film, a thin micellar solution film is formed. As the thickness of the liquid thin film decreases to a critical value due to evaporation of the solvent, holes open to restore the film to its equilibrium thickness [28]. When the holes grow larger due to evaporation-driven instability, the moving contact line works as a sink to collect the micelles by capillary flow and sweeping [30]. As a result, the solvents and spherical micelles are "pushed out" into the rim of the advancing holes. When the outward radial force is no longer sufficient to overcome the frictional effects of the micelles, which are collected in the rim, the advance of the rim of the growing holes stops [31].

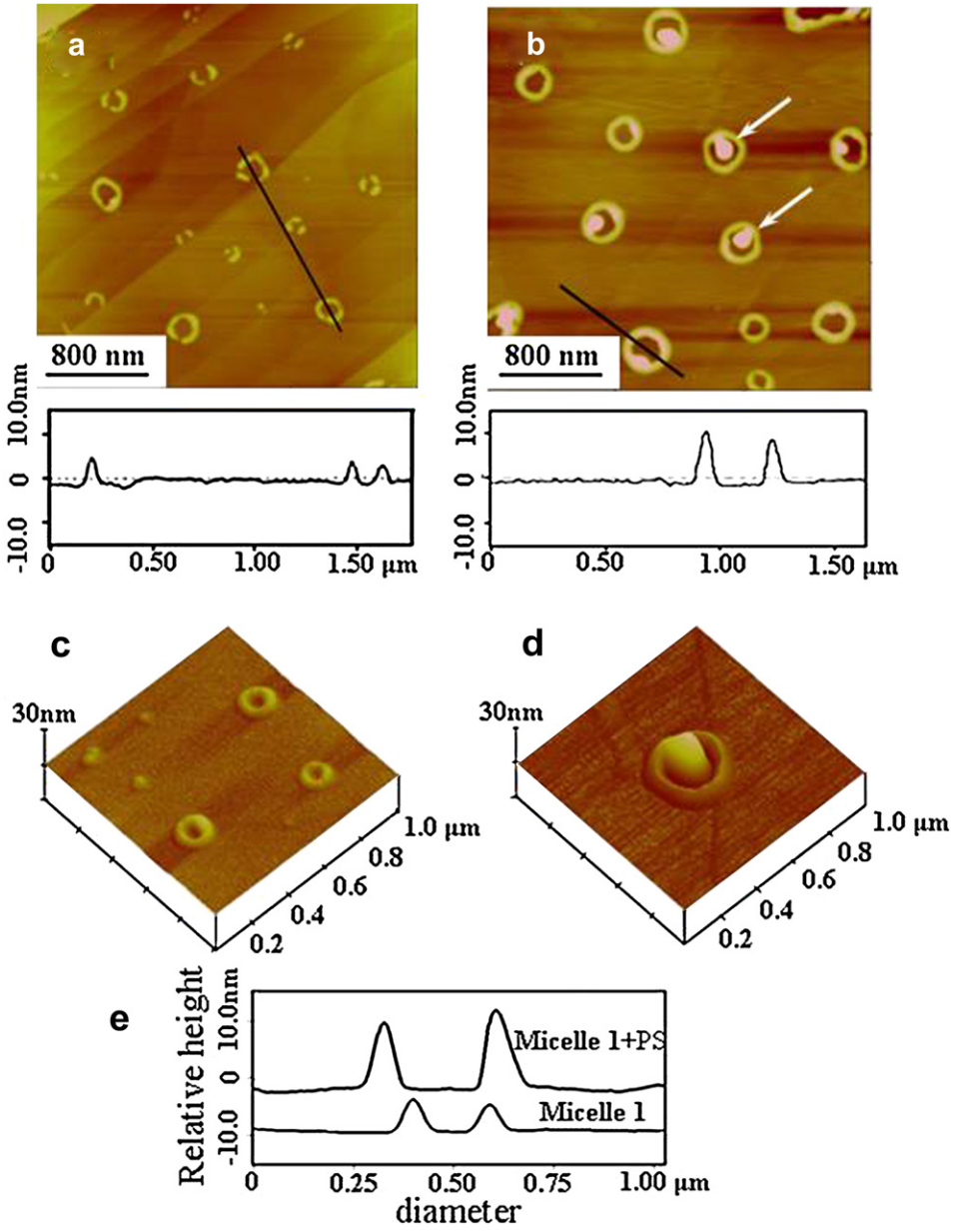

Fig. 2. AFM height images showing aggregations of **Micelle 1** (a) without any additive; (b) with addition of PS. AFM 3D height images showing nanorings of **Micelle 1** (c) without any additive and (d) with the addition of PS. (e) An AFM cross-section of the rings of **Micelle 1** and **Micelle 1** with the addition of PS. The contrast in (a) and (b) indicates a height variation from 0 to 30 nm. The samples were prepared using spin-coating method.

Nanorings, as shown in Fig. 1c, are then obtained by draining the rest of the solution.

We assumed that the observed large compound micelles in the same film were correlated with the thickness of the liquid film, which was determined by the size of the droplet used on the TEM grid or the HOPG substrate. Through systematic studies, we found that the thickness of the liquid film plays a critical role in the resulting morphologies: (i) thick liquid films generally induce the formation of large compound micelles; (ii) thin liquid films favor the formation of nanorings; and (iii) films with intermediate thicknesses generate a mixture of nanorings and large compound micelles. In thick liquid films, holes rarely formed during the dissipative dewetting process, such that micelles aggregated to form only large compound micelles. On the other hand, holes can be formed easily during the dewetting process when the liquid film is relatively thin. Another possible explanation is that a thicker liquid film contained more micelles and it cannot form single molecular layer after being dried. As long as a small cluster formed, the micelles aggregated and started to attract more micelles due to Ostwald ripening.

A high-resolution TEM micrograph in the inset of Fig. 1c reveals the structural details of the toroidal perimeter, showing the absence of rifts in the rim. We thus speculated that the surface of the rings is covered by a layer of PS and that the stresses inside the rings should be much higher than those on the outside. To confirm this assumption, we mixed 20 μL of PS homopolymer ($M_w = 24000$ g/mol, PDI = 1.06, purchased from Polymer Source Inc.) toluene solution at 10.0 mg/mL with 1 mL of the **Micelle 1** (0.20 mg/mL) solution. If we neglected a small volume change, the concentration of the PS homopolymer in the final mixture remained at 0.20 mg/mL. DLS measurements showed two peaks centered at 4.4 and 43 nm, corresponding to hydrodynamic radii of PS homopolymer random coils and PS_{385}-*b*-PAA_{154} spherical micelles, respectively. AFM height images, as shown in Fig. 2, reveal that a mixture of **Micelle 1** and PS forms nanorings from liquid films. When PS was added, the height, thickness, and outer radius of the rings increased significantly from 5, 70 and 135 nm to 9, 90, and 195 nm, respectively. These results indicated that the surface of the rings is covered by PS blocks because the added PS increased the thickness of the outer PS layer of the rings. Moreover, it is of interest to note that the phase separation between the PS homopolymer and the PS blocks of PS_{385}-*b*-PAA_{154} occurred only inside the rings, as indicated by arrows in Fig. 2b. The reason is that the PS segments of PS_{385}-*b*-PAA_{154} were tethered at the interface between the PS and PAA domains. The reduction of the mixing entropy caused the demixing of the PS homopolymer from the PS coronal regimes as the solvent evaporated because the PS chain density from the PS-*b*-PAA copolymer was much higher than that on the outside rings.

We sought to determine what would happen if we reversed the spherical micellar structure with PS as the micellar core and PAA as the micellar corona, by using a different solvent. We processed the diblock copolymer in a same way while using water as the solvent to induce micelle formation from the DMF solution followed by exhaustive dialysis to remove the cosolvent, DMF. In this case, **Micelle 2** with PS as its core and PAA as its shell was formed. Fig. 3a, which shows a TEM micrograph of the micelles formed by the freeze-drying method, reveals that PS_{385}-*b*-PAA_{154} formed spherical micelles (**Micelle 2**) with radius of 39 nm. DLS results gave an average radius of 63 nm (see supporting information, Fig. S2). PS_{385}-*b*-PAA_{154} forms so-called crew-cut micelles because the PAA blocks as a shell are much shorter than the PS blocks. We removed the water using the spin-coating method and found that the PS_{385}-*b*-PAA_{154} spherical

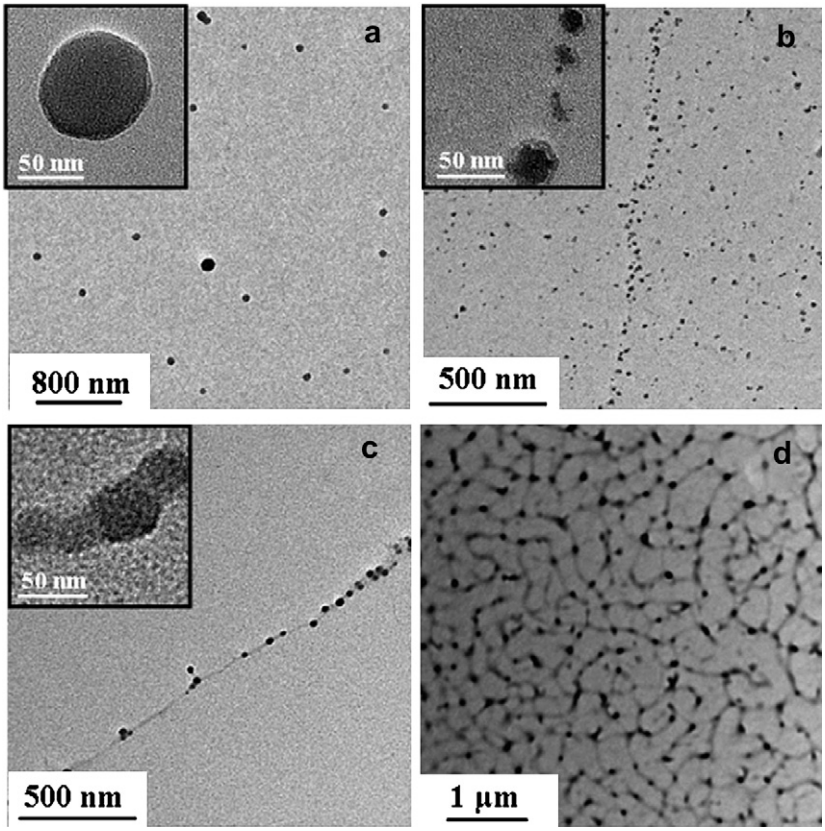

Fig. 3. TEM micrographs showing the re-assembly of **Micelle 1**. (a) Spherical micelles. (b) Intermediate stages of nanowires. (c) Nanowires. (d) Networks. Samples were prepared (a) using freeze-drying method and (b) to (d) using spin-coating method.

micelles re-assembled into distinguishable necklace-like objects as the water evaporated at room temperature. It is worth noting that the spherical micellar structure was presumably frozen because the PS, which has a much higher T_g than room temperature, was the micellar core material [2,20,32]. All intermediate micellar morphologies at different stages could be captured by TEM and AFM. Fig. 3b and c shows the progressive evolution of the aggregate morphology, which changed from crew-cut micelles to strings of micelles and then to necklace-like aggregates. Fig. 3b shows the formation of strings of micelles at a high spin-coating rate (4000 rpm). A decrease in the spin-coating rate (2000 rpm) resulted in the formation of one-dimensional necklace-like aggregates, as shown in Fig. 3c (see also supporting information, Fig. S3c). A careful examination of TEM results, as shown in Fig. 3b, revealed that the spherical micelles are very close to each with gaps between the neighboring micelles. The dark and gray areas, shown in the inset of Fig. 3b, represent the PS cores and PAA coronas, respectively. A further decrease in the spin-coating rate (1300 rpm) caused the formation of a network-structure, as shown in Fig. 3d (see also supporting information, Fig. S3d). TEM (c.f., Fig. 3b–d) and AFM (c.f., Fig. S3 b–d) results both clearly demonstrate the progressive evolution of the re-assembled structures under different spin-coating rates. The radius of an individual string was measured to be about 26 nm (c.f., Fig. S3d), which is consistent with the radius of the individual crew-cut micelles. Compared to micelles produced with the freeze-drying method (c.f., Fig. 3a), the micelles produced with the spin-coating method were slightly smaller due to the collapse of the dehydrated PAA shell.

This re-assembly phenomenon from spherical micelles was surprising, considering that the nanostructures of **Micelle 2** are kinetically frozen due to the glassy PS core [2,20,32]. The free energy contributions in diblock copolymer self-assembly systems are well known. It has been suggested [20,33] that the free energy balance from forming such aggregates of PS-*b*-PAA diblock copolymers generally involved three factors, i.e., the deformation (stretching) of the PS blocks in the core, the interfacial tension between the core and the solvent and the interactions among the coronal chains. The free energy contribution from the PS domains and the interfacial tension should be minimal during the re-assembly of PS-*b*-PAA spherical micelles because the hydrophobic PS core is glassy and rigid. Thus, a reasonable driving force for the post-micellization morphology transition could be caused by the specific interactions, such as hydrogen bonding, among the PAA chains (c.f., Scheme 2). In the aqueous solution, the **Micelle 2** surface is covered with the extended PAA segments, which were partially dissociated and ionized [34]. During the water evaporation process, the dissociation of the carboxyl groups became weaker, thus decreasing the carboxylate anion content and increasing the non-charged PAA block content. This process is accompanied by a shortening of the distance between the micelles. As more water evaporates, the gaps between the neighboring micelles become small enough for the formation of hydrogen bonds to occur between the neighboring micellar shells. Once hydrogen bonds are formed, they change the intramicellar interactions from repulsive to attractive. With the increasing fraction of the non-charged PAA blocks and the formation of more hydrogen bonds between the micelles, the PAA blocks become less soluble. Consequently, more micelles precipitate from the water and finally aggregate to form nanowires, as shown in Fig. 3. The combination of the neighboring micellar PAA shells produces a block copolymer re-assembly pathway, resulting in the one-dimensional growth of the spherical structures into long nanowires up to microns in length.

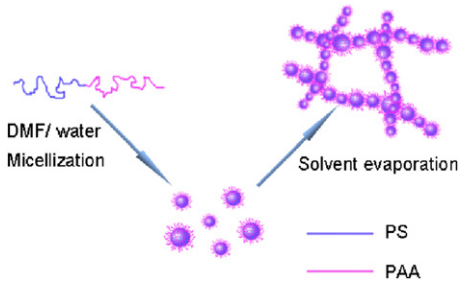

Scheme 2. Diagram showing the proposed mechanism for re-assembly of **Micelle 2** into networks.

Micelle 2 could not re-assemble into nanorings under the same experimental conditions. Instead, spheres, necklace-like structures and networks were observed (c.f., Fig. 3). In contrast to results reported in the literature [3,9,22], this was initially surprising because a change in the solvent can generate a variety of aggregate morphologies re-assembled from soft nanoparticles. Based on our results, the chemical composition of the core and corona as well as the interactions between the environment and the corona are the major factors for the different re-assembly behaviors observed in **Micelles 1** and **2**. Another possible reason is the specific interactions between PS or PAA and the HOPG substrate. The precise mechanism is still under investigation.

4. Conclusion

We discovered an alternative method to develop supramolecular structures through the re-assembly of spherical micelles. Our results demonstrated that re-assembly of spherical micelles of PS_{385}-*b*-PAA_{154} can be tuned by the selection of a solvent with an appropriate evaporation rate. With a solvent for PS, such as toluene, the soft spheres can re-assemble into nanorings and large compound micelles depending on the thickness of the liquid film. The underlying mechanism can be explained as a hole-nucleation and -growth process induced by dewetting. With a solvent for PAA, such as water, necklace-like assemblies and networks can be obtained using different spin-coating speeds. We found that the chemical identities of the micellar corona played a critical role in terms of the aggregate morphology evolution during the re-assembly of spherical micelles.

Acknowledgments

This work was financially supported by the National Basic Research Program of China (973 program, Grant 2007CB936400), the National High Technology Research and Development Program of China (863 Program, Grant 2009AA03Z229, 2008AA11A101) and the National Natural Science Foundation of China (Grant 20634050, 20804053, 50521302).

Appendix. Supplementary data

Supplementary data associated with this article can be found in the online version, at doi:10.1016/j.polymer.2009.10.031

References

[1] Whitesides GM, Boncheva M. Proc Natl Acad Sci U S A 2002;99:4769.
[2] Zhang L, Eisenberg A. Science 1995;268:1728.
[3] Yu K, Zhang L, Eisenberg A. Langmuir 1996;12:5980.
[4] Raez J, Manners I, Winnik MA. J Am Chem Soc 2002;124:10381.
[5] Jain S, Bates FS. Science 2003;300:460.
[6] Jenekhe SA, Chen XL. Science 1998;279:1903.
[7] Liang GD, Xu JT, Fan ZQ, Mai SM, Ryan AJ. Polymer 2007;48:7201.
[8] Jenekhe SA, Chen XL. Science 1999;283:372.
[9] Plestil J, Hlavat D, Hrouz J, Tuzar Z. Polymer 1990;31:2112.
[10] Mao BW, Gan LH, Gan YY, Tam KC, Tan OK. Polymer 2005;46:10045.

[11] Perreur C, Habas J-P, Lapp A, Peyrelasse J. Polymer 2006;47:841.
[12] Pietsch T, Gindy N, Fahmi A. Polymer 2008;49:914.
[13] Li ZB, Kesselman E, Talmon Y, Hillmyer MA, Lodge TP. Science 2004;306:98.
[14] Tsitsilianis C, Stavrouli N, Bocharova V, Angelopoulos S, Kiriy A, Katsampas I, et al. Polymer 2008;49:2996.
[15] Gohy JF. Adv Polym Sci 2005;190:65.
[16] Cui H, Chen Z, Zhong S, Wooley KL, Pochan DJ. Science 2007;317:647.
[17] Nikolic MS, Olsson C, Salcher A, Kornowski A, Rank A, Schubert R, et al. Angew. Chem. Int. Ed. 2009;48:2752.
[18] Yang XQ, Chen YH, Yuan RX, Chen GH, Blanco E, Gao JM, et al. Polymer 2008; 49:3477.
[19] Zheng R, Liu G, Jao TC. Polymer 2007;48:7049.
[20] Zhang L, Eisenberg A. J Am Chem Soc 1996;118:3168.
[21] Davis KA, Matyjaszewski K. Macromolecules 2000;33:4039.
[22] Xie DH, Xu K, Bai RK, Zhang GZ. J Phys Chem B 2007;111:778.
[23] Bunz UHF. Adv Mater 2006;18:973.
[24] Gong Y, Hu Z, Chen Y, Huang H, He T. Langmuir 2005;21:11870.
[25] Zhu J, Liao Y, Jiang W. Langmuir 2004;20:3809.
[26] Pochan DJ, Chen Z, Cui H, Hales K, Qi K, Wooley KL. Science 2004;306:94.
[27] Maillard M, Motte L, Ngo AT, Pileni MP. J Phys Chem B 2000;104:11871.
[28 Ohara PC, Heath JR, Gelbart WM. Angew Chem Int Ed Engl 1997;36:1078.
[29] Schenning APHJ, Benneker FBG, Geurts HPM, Liu XY, Nolte RJM. J Am Chem Soc 1996;118:8549.
[30] Suematsu NJ, Ogawa Y, Yamamoto Y, Yamaguchi T. J Colloid Interface Sci 2007;310:648.
[31] Zhou WL, He JB, Fang JY, Huynh TA, Kennedy TJ, Stokes KL, et al. J Appl Phys 2003;93:7340.
[32] Zhang L, Shen H, Eisenberg A. Macromolecules 1997;30:1001.
[33] Zhang L, Eisenberg A. Macromolecules 1996;29:8805.
[34] Zhang L, Barlow RJ, Eisenberg A. Macromolecules 1995;28:6055.